

# An electromagnetic coupling treatment for improving the cutting performance of cemented carbide-coated tools

Kaiken Sun<sup>a,b</sup>, Bo Zeng<sup>a,b</sup>, Yi Qin<sup>c</sup>, Chengjun Deng<sup>a</sup>, Yi Yang<sup>a</sup>, Kunlan Huang<sup>a,b</sup> and Jie Wang<sup>a,b</sup>

<sup>a</sup>School of Mechanical Engineering, Sichuan University, Chengdu, Sichuan, P.R. China; <sup>b</sup>Yibin Industrial Technology Research Institute of Sichuan University, Yibin, Sichuan, P.R. China; <sup>c</sup>Centre for Precision Manufacturing, DMEM, The University of Strathclyde, Glasgow, UK

## ABSTRACT

To improve the cutting performance and prolong the service life of a carbide-coated tool in the process of ductile iron machining, an electromagnetic coupling treatment (EMCT) was carried out. The cutting experiments show that the cutting force and cutting temperature are reduced after EMCT, and the roughness of the machined surface is reduced. It is found that after EMCT with optimal parameters the dislocation density, microscopic strain, microhardness and bonding strength of an alumina coating increase by 109.2%, 28.2%, 28.3% and 26.6%, respectively. Using the actual machining of a differential housing to verify the tool life, it is found that after EMCT, a single tool can process 18.4 more workpieces or in other words, the tool life increased by 44%. EMCT can promote element diffusion, optimize coating properties and have great potential in coating tool life extension.

## ARTICLE HISTORY

Received 29 March 2023

Accepted 12 September 2023



## KEYWORDS

Electromagnetic coupling treatment; carbide-coated tool; cutting performance; adhesion strength; diffusion

## 1. Introduction

Ductile iron is widely used in wear-resistant parts such as a diesel engine body, cylinder head and crankshaft due to its prominent casting performance, corrosion resistance, wear resistance and vibration reduction. Ductile iron accounts for more than 40% of the cast iron market today [1]. But ductile iron is difficult to process because of its high hardness and strength. Especially pearlite ductile iron, its strength is higher, but machining tool life is significantly reduced [2]. The dispersed matrix structure of ductile cast iron is the main factor affecting its machinability. The hard phase in ductile cast iron will impact the tool and affect the stability of the cutting process and tool life [3]. Chip discontinuity will increase tool vibration and wear, while heat accumulation in the tool nose will accelerate the oxidation and failure at that point. If the more expensive CBN cutting tool is used, the ferrite in cast iron will cause chemical erosion of the CBN particles in the tool, resulting in rapid wear and reduced tool life [4,5]. Currently, coated cemented carbide tools with good wear resistance and oxidation resistance are mainly used for processing [6–8], but there are still some problems, such as short tool life and poor surface quality [9]. It is therefore necessary to find a way to enhance the cutting performance of coated cemented carbide tools, so as to improve the machining quality and prolong the tool life [10].

Electromagnetic coupling treatment (EMCT) is one of the special energy field assisted manufacturing technologies. The technology is used to strengthen metal parts by coupling applied pulsed electric and magnetic fields in order to obtain modifications by adjusting the material microstructure [11]. This technology offers the advantages of being quick to process, having a clear result and not polluting the environment. It is a brand-new tool that advances technology [12]. A large amount of studies have found that the external magnetic field will affect the microstructure of materials and thus change their properties [13]. Yongfeng Yang conducted magnetic treatment on a cemented carbide (WC-12Co) milling tool, and found that the cutting process changed from two-body friction to three-body friction, thus the wear resistance was improved. Moreover, magnetic field treatment causes dislocation movement and improves tool hardness [14,15]. Qiuqin Li applied pulsed magnetic field treatment to a WC-6Co tool and carried out cutting experiments on TC4 with the treated tool, and found that the life of the tool was prolonged and the surface quality of the workpiece was enhanced [16]. Li's research shows that magnetic field treatment improves tool thermal conductivity and improves wear performance. Hao Qiu applied pulse magnetic treatment to the coated tool and carried out cutting experiments,

**CONTACT** Kunlan Huang  huangkunlan@scu.edu.cn  School of Mechanical Engineering, Sichuan University, South 1st Section of 1st Ring Road, Chengdu, Sichuan 610065, China

© 2023 The Author(s). Published by Informa UK Limited, trading as Taylor & Francis Group on behalf of The Korean Ceramic Society and The Ceramic Society of Japan. This is an Open Access article distributed under the terms of the Creative Commons Attribution License (<http://creativecommons.org/licenses/by/4.0/>), which permits unrestricted use, distribution, and reproduction in any medium, provided the original work is properly cited. The terms on which this article has been published allow the posting of the Accepted Manuscript in a repository by the author(s) or with their consent.

and found that the residual compressive stress of the coating increased, the adhesion improved, and the tool life prolonged [17]. Hanlin Fei carried out pulsed magnetic field treatment on a CBN tool, and the cutting experiment found that after the treatment flank wear of the tool was greatly reduced [18]. Fei's research suggests that pulsed magnetic field treatment can increase the compressive stress and bonding strength of the coating. Studies have shown that electric fields can promote atomic diffusion and defect repair of metal materials [19,20]

An external magnetic field superimposed with an electric field will produce a more significant change in the performance of the metal material. Qianwen Zhang found that an electromagnetic coupling treatment can improve the thermal conductivity of WC-8Co [21], Min Yuan found that the electromagnetic coupling treatment can improve the fracture toughness and reduce the cutting heat of WC-TiC-Co cermet tools [22]. Existing studies have shown that electromagnetic coupling treatment can optimize the properties of cemented carbide materials and extend the cutting life, but there are few reports on how to improve the mechanical performance of coated cemented carbide tools.

In this paper, an electromagnetic coupling treatment is used to treat coated carbide tools for machining ductile iron, with the aim of studying the mechanical and cutting properties of coated carbide after the treatment and exploring the strengthening mechanism of the mechanical properties.

## 2. Materials and methods

### 2.1. Coated carbide tool

The substrate of the tool (CNMG120412-RK MC5015, Mitsubishi, Japan) used in this experiment is WC-8Co, with a transition layer of 9.7  $\mu\text{m}$  TiCN and the outer layer of 4.8  $\mu\text{m}$   $\text{Al}_2\text{O}_3$  coating. The SEM image and EDS information of the carbide coated tool are shown in Figure 1.

### 2.2. Workpiece materials

The material used in the cutting experiment is the pearlite ductile iron bar of QT600-3 with a diameter of 70 mm and a length of 200 mm. Its chemical composition is shown in Table 1. In the actual production process, this blade is used to process the housing of a certain type of differential, and the material is also QT600-3. The photos of the ductile iron bar and the differential gear housing are given in Figure 2.

### 2.3. Electromagnetic coupling treatment (EMCT)

Figure 3 is a schematic diagram of the electromagnetic coupling field generator used in this experiment. Copper electrodes are connected to both sides of the sample, and a pulsed current is applied. The excitation coil provides a spatial magnetic field. Current power supply and excitation coil power supply work synchronously through PLC control. When the magnetic pulse is released, the current pulse is applied to realize the electromagnetic coupling of the sample.

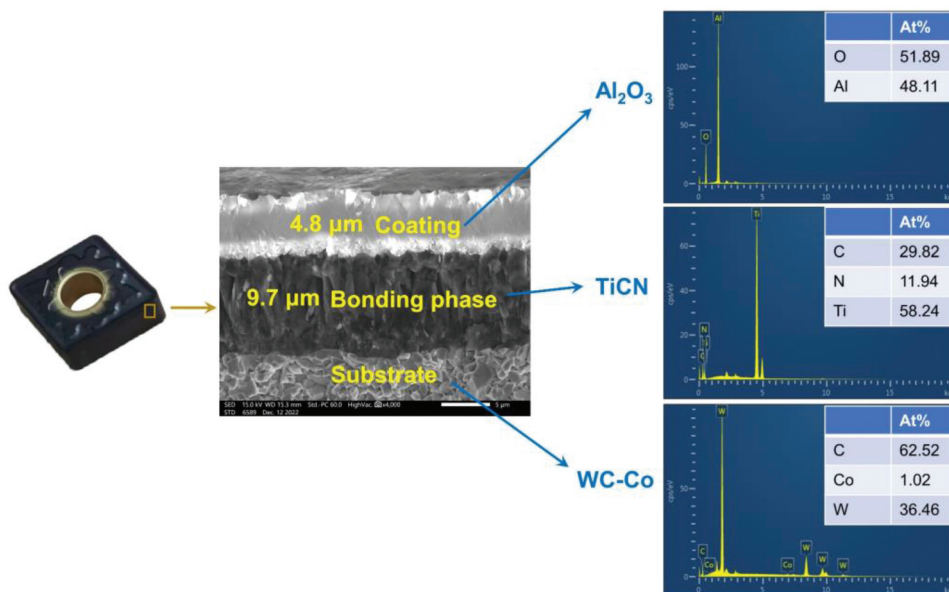
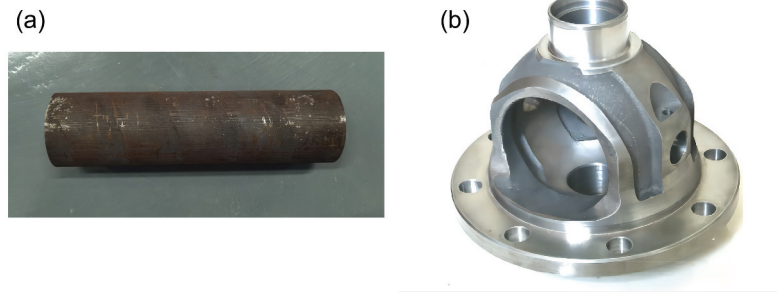


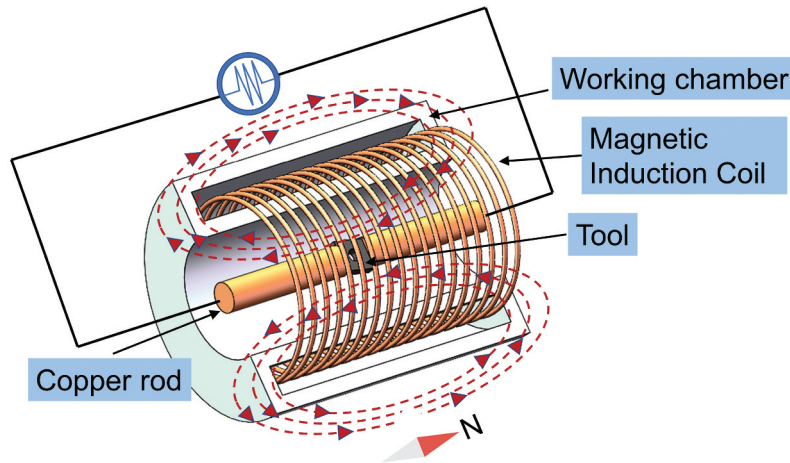
Figure 1. SEM images with EDS analysis of the tool.

Table 1. Element composition of QT600-3.

Elements	C	Si	Mn	S	P	Mg	Fe
Wt.%	3.7	2.5	0.35	0.03	0.07	0.05	Balance



**Figure 2.** Cast iron bar used in cutting experiment (a) and differential gear housing in actual machining (b).



**Figure 3.** Schematic diagram of the electromagnetic coupling treatment.

**Table 2.** Processing parameters of electromagnetic coupling treatment.

Treatment	Number of specimens				
	Tool 1	Tool 2	Tool 3	Tool 4	Tool 5
Magnetic field intensity (T)	0	0.5	1.0	1.5	2.0
Magnetic field frequency (Hz)	0	1.0	1.0	1.0	1.0
Electric field intensity (V)	0	1.2	1.2	1.2	1.2
Electric field frequency (Hz)	0	50	50	50	50
Processing time (min)	0	4	4	4	4
Processing temperature (°C)	25	25	25	25	25

Previous experiments demonstrate that the electric field provided by the current and the magnetic field provided by the excitation coil will affect the performance of the sample in varying degrees. The electric field intensity and magnetic field intensity are two variables of this experiment, and the experimental parameters are set as shown in Table 2. Among them, Tool 1 was the control sample.

#### 2.4. Cutting experiment

In order to study the impact of EMCT on the cutting performance of coated cutting tools, dry cutting experiments were carried out on a CK6140 CNC machine with the above-mentioned numbered cutting tools (Figure 4). The cutting parameters were as follows: spindle speed 400 r/min, cutting depth 0.5 mm, feed speed 0.2 mm/r. The distance of each

axial feed is 130 mm, and the feed process is repeated 13 times until the workpiece diameter is reduced to 45 mm. During the cutting process, a Kistler 9257B three-way dynamometer was used to collect cutting force data, and the sampling frequency was 800 Hz. The cutting temperature is measured by a FLIRA 655SC thermal imager (FLIR, USA).

#### 2.5. Actual machining verification

To further verify the cutting performance of the tool after EMCT, tool was used in the actual production to process the differential housing. The tool life is evaluated based on the maximum number of pieces processed, and the machining quality is evaluated by the surface roughness of the workpiece.

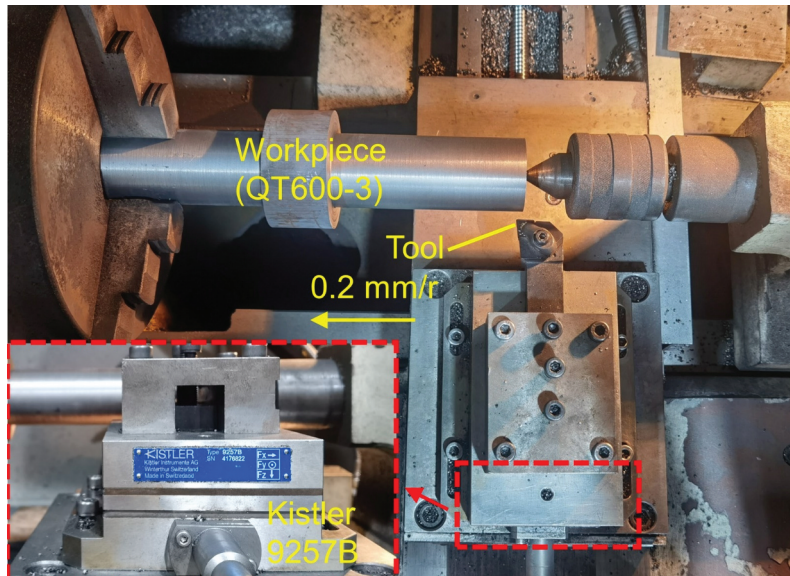


Figure 4. Turning experiment set up.

## 2.6. Measurement

The tool wear was measured by a VSM-3020 optical profilometer. A Bruker Contour GT-K was used to measure the surface roughness of the workpiece. A Nano Indenter G200 was used to measure the nanohardness and elastic modulus of the tool coating at a pressure of 8 mN. The bond strength of coatings was measured by an Anton Paar Rst automatic scratch instrument with a loading speed of 198 N/min. The tool section morphology was observed with a Thermo Scientific™ Apreo S emission scanning electron microscope, and elemental analysis was performed with the Oxford X-Max energy spectrum detection system mounted with the electron

microscope. The thermal conductivity of the tool as a whole is measured in this study. The shape of the tool is a rhombus. A pair of parallel planes are selected as the test surface. The device LW-9389 is used for testing according to the ASTM 5470 standard, and multiple measurements are averaged to get the final result.

## 3. Results and discussion

### 3.1. Cutting force

Figure 5 shows the feeding force ( $F_x$ ), radial thrust force ( $F_y$ ), tangential force ( $F_z$ ) and resultant force of the tools after EMCT with different parameters in the

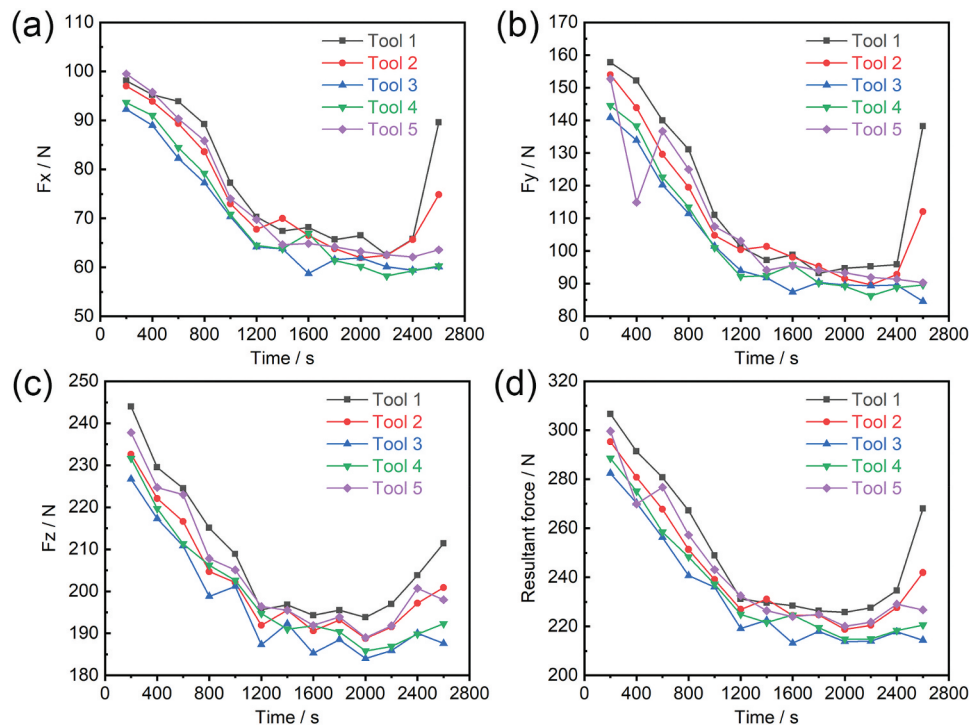


Figure 5. Cutting forces of tools under different EMCTs: (a)  $f_x$ , (b)  $f_y$ , (c)  $f_z$ , (d) resultant force.

cutting experiment, where Tool 1 represents the control group, which is the original tool without EMCT. As can be seen from the figure, with the extension of cutting time, the cutting force in the three directions and resultant force gradually decrease and become stable. When the cutting time exceeds 2200 s, the cutting forces of Tool 1 and Tool 2 start to increase abruptly, which may be because the flank of the tool is continuously worn and consumed in the cutting experiment and the coating begins to fail [23]. Compared with Tool 1, the tools after EMCT show a lower level of cutting force and a longer stable cutting time, which may be related to the hardness and wear resistance of the tools' coatings [24]. Among them, in all cutting experiments, the cutting force of Tool 3 is the smallest, and at 2600 s is still stable, indicating that the tool wear is still slight at this time and is not at the failure state.

### 3.2. Cutting temperature and thermal conductivity

The cutting temperature has a great influence on the tool life and workpiece surface quality. Continuous high temperature cutting easily leads to tool failure. Studying the changing laws of cutting temperature can provide effective information for analyzing tool life and machining quality. In the process of cutting, the cutting tool and the cutting material experience friction at high speed, resulting in considerable cutting heat. Some of the heat is carried away by the chip, and some is absorbed by the nose of the tool and carried backwards. If the thermal conductivity of the tool is poor, it is easy to lead to the accumulation of heat in the tool nose, which increases the tool's thermal deformation and wear consumption, shorten the tool's life, and affects the surface roughness of the machined object [25].

The cutting temperature was recorded by an infrared thermal imager. Figure 6 shows the temperature trend from tool nose to body during steady cutting. The horizontal axis represents the distance between the test point and the tool nose (mm), and the

vertical axis represents the temperature ( $^{\circ}\text{C}$ ). As can be seen from the figure, the temperature gradually decreases from the nose to the body of the tool. Lower tool nose temperatures for Tools 2 through 5 than for Tool 1 may be due to the EMCT, which lessens friction and heat generation during tool cutting [21,25]. Tool 1 has the steepest line, while Tool 3 has a more gentle slope, which reflects the difference in thermal conductivity of different samples. The thermal conductivity determines how easily the heat from the nose can be transferred backwards. Tool 1 and Tool 3 with the largest trend difference were selected for the thermal conductivity test, and the results are shown in Table 3. It can be seen that after the EMCT with magnetic field intensity 1.0 T and electric field intensity 1.2 V, the tool's thermal conductivity is increased from 8.86 W/(m·K) to 9.47 W/(m·K), an increase of 6.9%. Therefore, after EMCT, the tool heat transfer is quicker, resulting in a smaller temperature differential between the tool's two ends, quicker heat dissipation at the tool nose, less accumulation of cutting heat, lower oxidation losses, and longer tool life.

### 3.3. Surface roughness

Surface roughness is a vital index to evaluate the quality of processed surface, which can reflect the wear behavior of the contact area between the cutting edge and the workpiece [26], and indirectly evaluate the life of the tool. In industry, average roughness (Ra) is mainly used to characterize the level of surface finish. The test results of the surface roughness of the experimental samples are shown in Figure 7.

The workpiece surface roughness acquired by the unprocessed Tool 1 is 4.08  $\mu\text{m}$ . However, the workpiece surface roughness acquired by the Tool treated with EMCT is reduced, and the value of the workpiece corresponding to Tool 3 is only 3.08  $\mu\text{m}$ . After EMCT, the wear of tip nose is reduced, so the workpiece surface roughness is smaller [26].

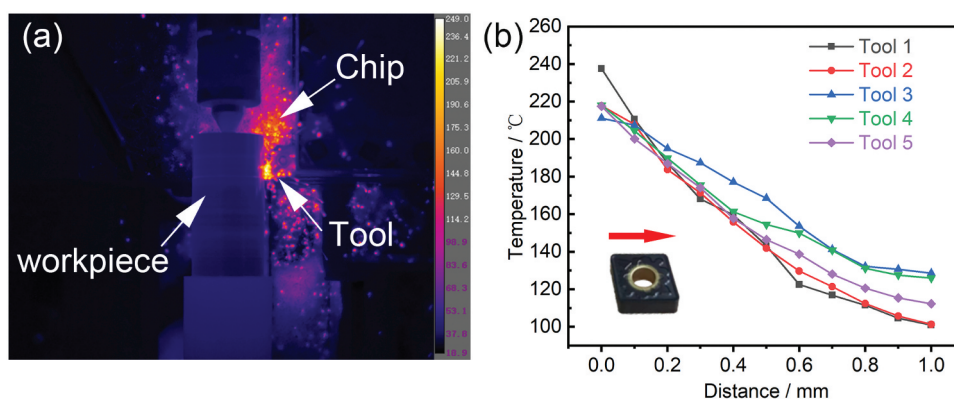


Figure 6. Photos of cutting temperature: (a) measurement, (b) temperature distribution of turning tool.

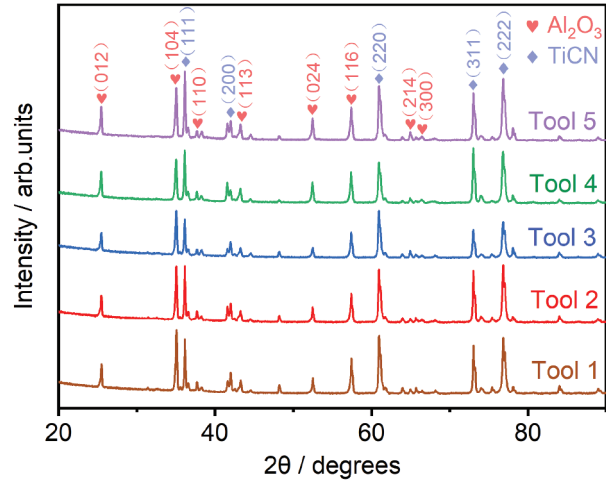
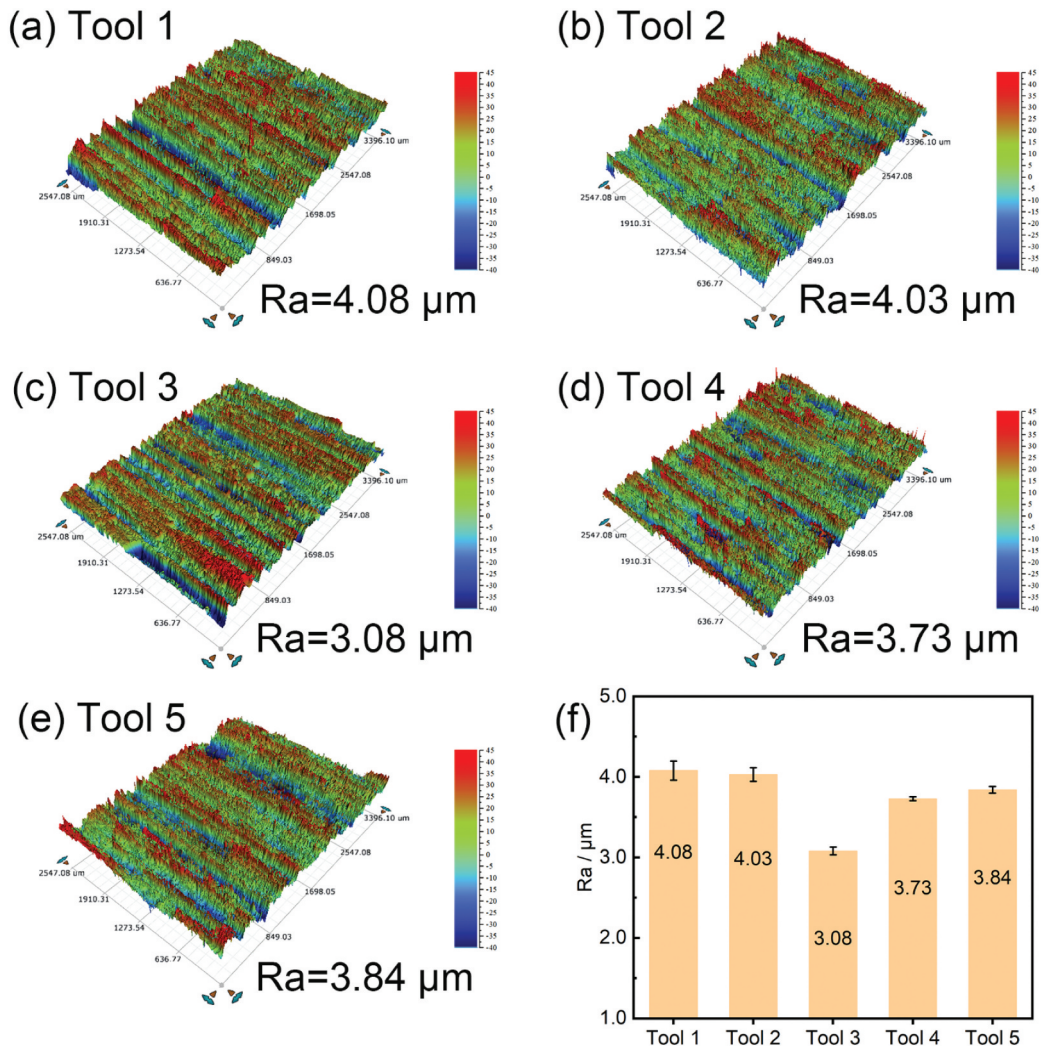
**Table 3.** Thermal conductivity results.

	Thermal conductivity W/(m·K)	Thermal diffusivity mm <sup>2</sup> /s
Tool 1	8.86	3.38
Tool 3	9.47	3.61

### 3.4. XRD analysis

The literature [27] shows that the performance and service life of coatings are affected by the difference in microstructure. Figure 8 shows the transition and outermost phases of the tool coating. This is because the XRD test depth is about 10  $\mu\text{m}$ , which is greater than the thickness of the outermost  $\text{Al}_2\text{O}_3$  (4.8  $\mu\text{m}$ ), so the inner bonding layer TiCN is also detected. The diffraction peaks of all samples did not shift, indicating that neither phase transformation nor generation of a new phase took place in the samples. In XRD data, the  $\text{Al}_2\text{O}_3$  diffraction peak with high diffraction intensity is selected and combined with Scherrer equation, the dislocation density ( $\delta$ ), microscopic strain ( $\epsilon$ ) and average grain size ( $D$ ) of each sample coating can be calculated [27]. According to the data of elastic modulus ( $E$ ) of  $\text{Al}_2\text{O}_3$  coating, residual stress can also be calculated.  $D$  is the coating average grain size (nm),

which can be obtained from Formula (1).  $\delta$  is the coating dislocation density ( $\text{nm}^{-2}$ ), which can be obtained from Equation (2).  $\epsilon$  is the microscopic strain calculated by Equation 5.  $\sigma$  is residual stress calculated by Equation 5., where  $k=0.89$  (Scherer constant),  $\lambda =$

**Figure 8.** XRD patterns of tools.**Figure 7.** Workpiece surface profiles (a–e) and roughness (f).

**Table 4.** Microstructure and properties of Al<sub>2</sub>O<sub>3</sub> coating.

Samples	D (nm)	E (GPa)	$\varepsilon \times 10^{-3}$	$\delta \times 10^{-3}$ (nm <sup>-2</sup> )	Stress (MPa)
Tool 1	37.58	224.95	2.487	0.747	559.5
Tool 2	35.95	220.52	2.589	0.841	571.0
Tool 3	30.25	247.40	3.189	1.561	789.0
Tool 4	30.35	245.63	3.110	1.356	763.9
Tool 5	32.36	236.96	2.862	1.013	678.1

0.15406 Å (Copper target),  $\beta$ =FWHM (radians),  $\theta$ =peak position (radians). The relevant data are shown in Table 4.

$$D = \frac{k\lambda}{\beta(\cos\theta)} \quad (1)$$

$$\delta = \frac{1}{D^2} \quad (2)$$

$$\varepsilon = \frac{1}{4 \tan \theta} \quad (3)$$

$$\sigma = \varepsilon E \quad (4)$$

It can be seen from the data in Table 4 that tool 3 has the highest microscopic strain, largest dislocation density and smallest grain size of Al<sub>2</sub>O<sub>3</sub> coating, while tool 1 has the opposite effect. The results show that the EMCT process increases the dislocation density (109.2%) and microscopic strain (28.2%) of the coating, and then increases the residual stress. According to the literature [18,28,29], the Al<sub>2</sub>O<sub>3</sub> coating should be in the state of compressive stress, and greater compressive stress is helpful to reduce the wear consumption of the coating and improve the service life.

### 3.5. Nanoindentation analysis

Figure 9(a) shows the load–displacement curves of five samples. According to the nanoindentation curve, the elastic modulus values (E), hardness (H) and elastic recovery rate can be calculated. The load–displacement curves of the same batch of cutters are obviously different after the EMCT with different parameters, which indicates that the mechanical performance of the coating is changed to different degrees during EMCT. The elastic recovery rate can be calculated from Equation 5.

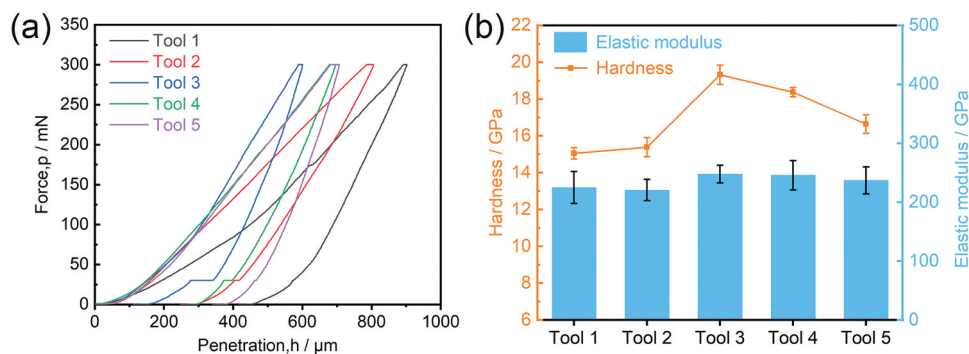
$$R_e = \frac{h_{\max} - h_f}{h_{\max}} \quad (5)$$

where  $h_{\max}$  represents the maximum displacement during loading, and  $h_f$  represents the displacement after unloading. Therefore, the coatings' Re values on the Tool 1 to Tool 5 were 53.80%, 69.35%, 81.55%, 64.50% and 54.60%, respectively. The higher the Re value of the material, the stronger the resistance to plastic deformation [30,31]. It can be seen from the calculation results that, compared with the control samples, the anti-plastic deformation ability of the tool coating is enhanced in different degrees after EMCT, and Tool 3 has the largest improvement.

Figure 9(b) shows the elastic modulus values and nanohardness of the five tools. As can be seen from the

**Table 5.** Micromechanical properties of five tools.

Samples	Elastic modulus (E)/GPa	Hardness (H)/GPa	H <sup>3</sup> /E <sup>2</sup>	H/E
Tool 1	224.95±45.63	15.05±0.62	0.0704	0.0680
Tool 2	220.52±67.87	15.38±0.96	0.0858	0.0731
Tool 3	247.40±51.84	19.31±0.98	0.1284	0.0801
Tool 4	245.63±63.19	18.38±0.64	0.1205	0.0783
Tool 5	236.96±33.57	16.64±0.96	0.0835	0.0707

**Figure 9.** Nanoindentation analysis: (a) load–displacement curve, (b) hardness and elastic modulus.

figure, after electromagnetic coupling treatment, the elastic modulus of the tool has no significant change, but the hardness has increased. The tool's initial hardness was 15.05 GPa, and it became harder after treatment. The most obvious is Tool 3, which reaches 19.31 GPa, up 28.3%. Table 5 shows the micromechanical properties of the sample measured by the nanoindentation experiment. As can be seen from the table, Tool 1 coating deformation resistance index ( $H^3/E^2$  and  $H/E$ ) is the lowest, while Tool 3 coating deformation resistance index is the highest. According to the plastic deformation theory, the greater the value of  $H^3/E^2$  and  $H/E$ , the stronger the anti-plastic deformation ability of the coating, that is, the coating tool has better wear resistance under load [32–34].

### 3.6. Adhesion strength

The bonding strength between coating and substrate is a significant index to evaluate coating quality, which

directly determines the cutting properties and service life of the coated tool. The adhesion strength of EMCT coatings with different parameters was measured by scratch method. In the scratching process, the sudden change of friction coefficient is taken as the signal that the coating is scratched, and the loading force at this time is the adhesion strength of the coating. Figure 10 shows a photograph of the scratch and the location of the friction coefficient mutation. As can be seen from the figure, the bonding strengths of Tool 1 to Tool 5 are 52.3 N, 59.4 N, 66.2 N, 65.5 N and 60.2 N, respectively. In other words, the tool coating's bonding strength is improved following EMCT to varying degrees, with a maximum rise of 26.6% (Tool 3).

The variation of bonding strength of the coating may be connected with the diffusion of elements between coating and substrate [27]. The enhancement of adhesion may be due to the enhanced diffusion process of elements between coatings. The failure of coating mostly rests with plastic deformation and fracture. In the early phase of the scratch experiment, the

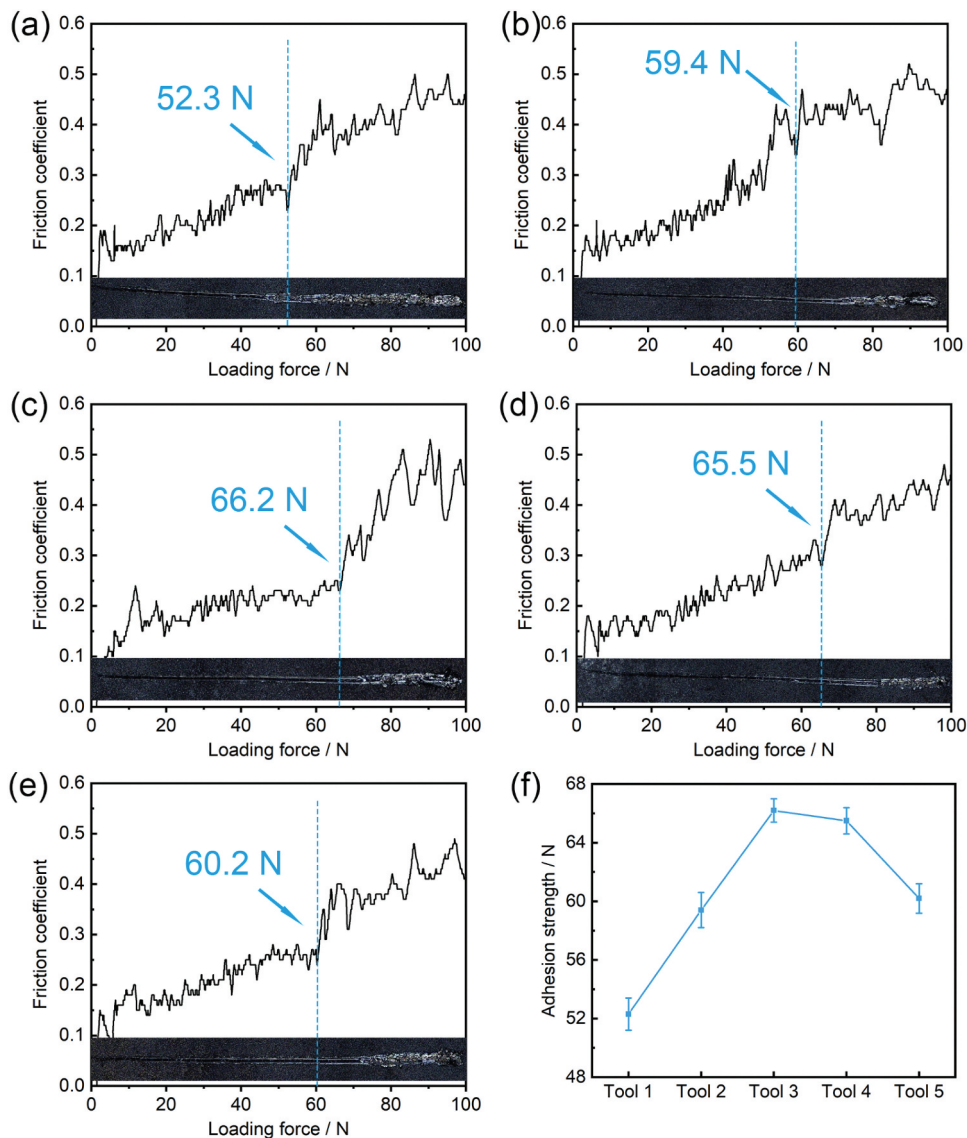


Figure 10. Scratch and friction coefficient: (a) tool 1, (b) tool 2, (c) tool 3, (d) tool 4, (e) tool 5, (f) adhesion of samples.



coating began to change from elastic deformation to plastic deformation. With the increase of the load, the coating was damaged until the applied load exceeded the plastic deformation limit of the coating when the coating was completely broken and spalling [35]. In the scratch experiment, the coatings' plastic deformation resistance is consistent with the results of nanoindentation analysis. After the EMCT with the electric field intensity of 1.2 V and the magnetic field intensity of 1.0 T, the bonding strength and plastic deformation resistance of the coating are improved.

The most immediate cause of increased adhesion strength is the diffusion of elements between coatings [36–38]. In order to further verify the effect of EMCT with electric field intensity of 1.2 V and magnetic field intensity of 1.0 T on the bonding strength of the tool coating, element distribution experiments in quasi-in-situ were carried out. An EDS line scan was performed on the specified location of the sample section first, and then the EMCT experiments of 1.2 V and 1.0 T were

conducted on the sample. Finally, an EDS line scan was performed again on the same location of the section, and the results are shown in Figure 8. The main focus is on the metal elements of the sample, which are Al, Ti and W, respectively. The area where the element content changes abruptly is the area of coating transition. Figure 11(b) shows that, before treatment, there is an element diffusion region of about 1.80  $\mu\text{m}$  between the outermost  $\text{Al}_2\text{O}_3$  and the bonding layer TiCN of the sample which is formed during the preparation of the coating. And a diffusion zone of 1.37  $\mu\text{m}$  thickness exists between TiCN and WC substrate.

After EMCT, the thickness of element diffusion region between  $\text{Al}_2\text{O}_3$  and TiCN increased to 2.01  $\mu\text{m}$  and that between TiCN and WC increased to 2.04  $\mu\text{m}$ . The variation indicating that the EMCT process promoted the element diffusion between coatings, enhanced the movement of aluminum in the outer alumina to the inner layer and enhanced the migration of Ti in the inner TiCN to the outer layer so does the Ti

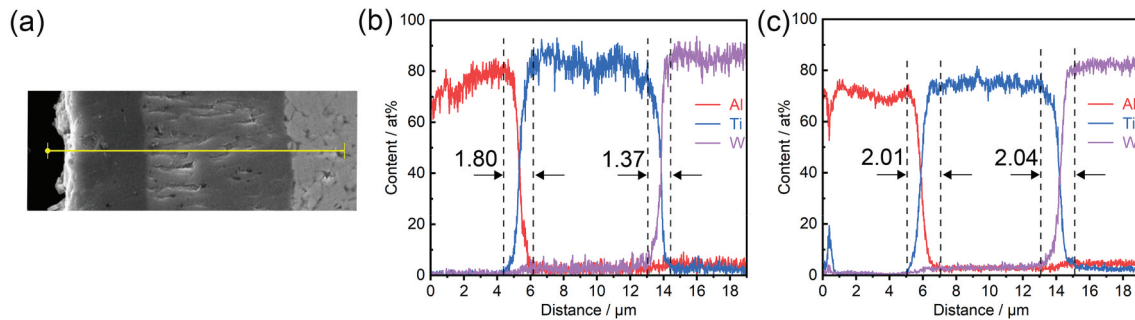


**Figure 11.** Quasi-in-situ EDS line scan photos of the sample: (a) cross-section SEM image, (b) elemental distributions before EMCT, (c) elemental distributions after EMCT.

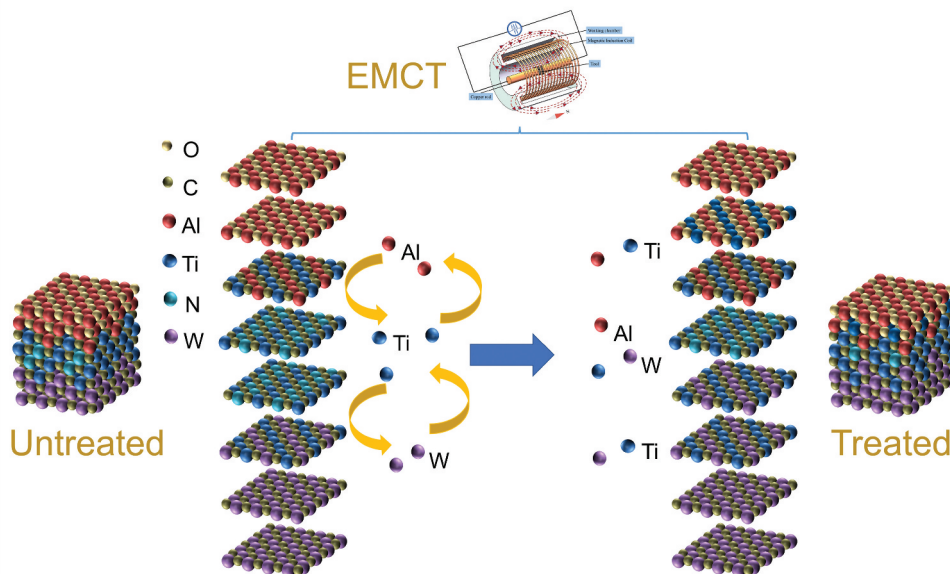


**Figure 12.** Schematic for the elements migration of the coatings.

and W in the next interface. Therefore, after EMCT with an electric field intensity of 1.2 V and magnetic field intensity of 1.0 T, two element diffusion gradient layers of about 200 nm and 700 nm were formed where the coating bonds, which improved the adhesion strength of the coating.

Figure 12 shows the migration of different elements in the tools during the EMCT process. The diagram on the left shows the initial state of the tool coating. The matrix is WC, the bonding layer is TiCN, and the outermost layer is Al<sub>2</sub>O<sub>3</sub>. The accumulation of atomic layers is a simple expression of coating thickness. At this time, there is a transition region between the outermost layer and the bonding layer, which is represented by the element mixing layer. There is also an element mixing layer between the bonding layer and the matrix, indicating the transition between TiCN and WC. During EMCT, elements begin to diffuse. Al in the outermost layer moves inward, while Ti in the middle layer also moves inward and outward, W in the matrix moves into TiCN layer. The result is an increase in the thickness of the mixing layer of elements, represented by two layers of atoms. The final coating obtained is shown in the right diagram. Compared with the initial state, the coating at this time has a greater thickness of the element diffusion gradient layer, which is of great significance for improving the binding strength, wear resistance and service life of the coating.

Under the action of the electric field, the disordered Al<sub>2</sub>O<sub>3</sub> molecules are no longer ionized but are turning direction polarization [39]. The orientations of electric dipoles tend to be uniform, and the O-Al bond is deflected directionally and elongated under the electric field, lowering the breakage energy of the O-Al bond [40]. In addition, due to the turning polarization, the electric dipole moment of the Al<sub>2</sub>O<sub>3</sub> molecule is not zero, and the atoms are in an unstable state, so that the O-Al bond is easy to break, helping the O atoms and Al atoms to diffuse into the inner TiCN. Under the conditions of an electric field, diffusion is a bidirectional process [41,42]. The magnetic field

will cause the movement of the free vacancy in the material organization, resulting in the lattice rearrangement of the microscopic region. Chemical bonds are formed and broken during structural rearrangement. The microscopic residual stress after fracture becomes the driving force of atomic migration [43]. Under the condition of electromagnetic coupling, the effects of electric field and magnetic field superposition promote each other, accelerate the fracture of the O-Al bond and the migration of Al and O atoms to the inner layer and finally realize element diffusion. The macroperformance is that the coating bonding force is enhanced and the cutting performance is markedly improved. The deeper theory of atomic migration between coatings during electromagnetic coupling treatment will continue to be explored in the following studies.

### 3.7. Tool life verification

The cutting experiments show that the cutting temperature, cutting force and surface roughness of workpiece are reduced after the EMCT. It is found that the EMCT can improve the hardness, plastic deformation resistance and bonding strength of the coating. However, whether the utility performance of the tool is improved must be tested through actual processing. The differential housing was processed with the tools that passed through the above EMCT, also numbered Tool 1 to Tool 5. After each machining of 10 pieces, the flank wear of the tools was measured (Figure 13), and the maximum machining life of each tool was noted. In order to evaluate the machining quality, the surface roughness of the 40th shell was observed and recorded (Figure 14).

The VB in Figure 13(a) shows the extent of tool wear. With the increase of the number of machining pieces, tool wear gradually intensifies. Compared with Tool 1, the wear extent of tools (Tool 2 to Tool 5) after EMCT is reduced. The blue line is the gentlest, indicating that

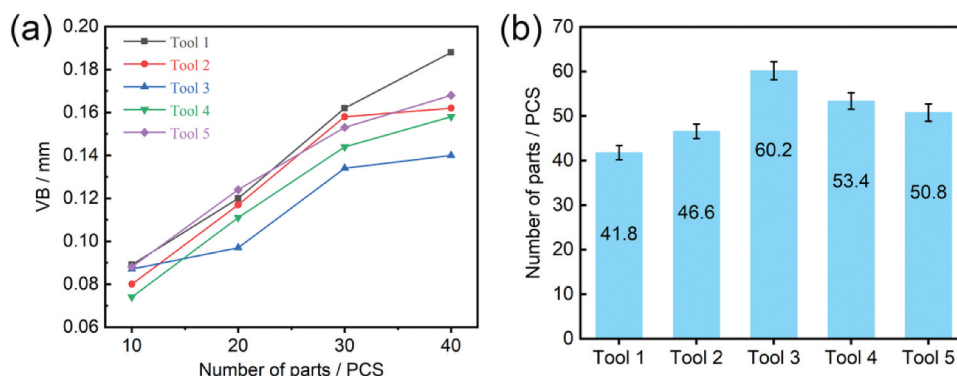


Figure 13. Tool life verification: (a) flank wear of tools, (b) maximum number of processed pieces.

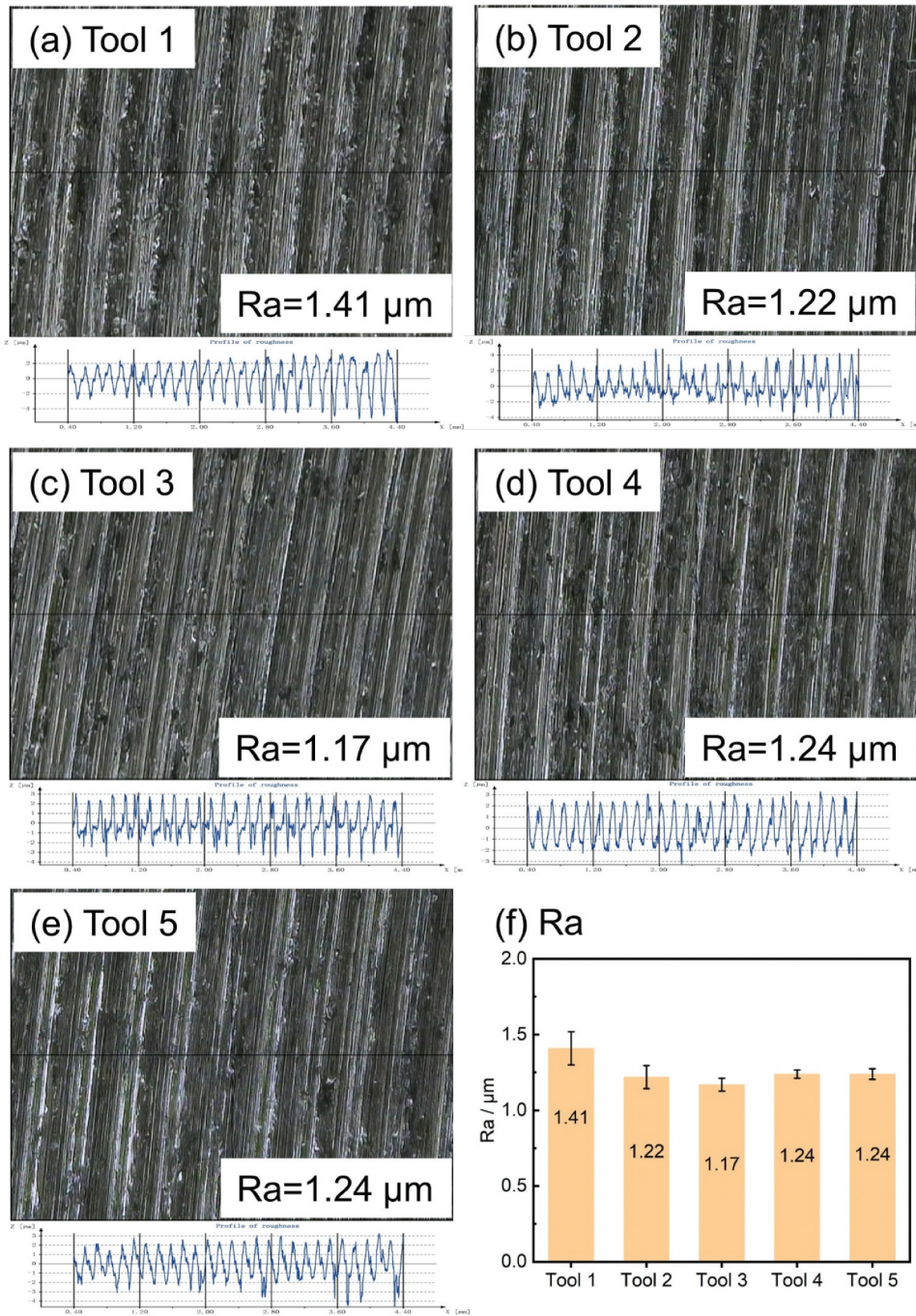


Figure 14. Surface roughness of number 40th differential housing.

Tool 3 has the lowest wear rate. After processing 40 workpieces, Tool 1's VB reaches 0.186 mm, while Tool 3's VB is only 0.141 mm, a 24.2% reduction. Reducing back tool wear is beneficial to prolong tool life and improve machining quality [44]. It can be seen from Figure 13(b), the maximum number of processed pieces of Tool 1 is only 41.8, while other tools are improved. The corresponding value of Tool 3 is 60.2, indicating that after EMCT of 1.2 V and 1.0 T, one tool can process 18.4 more workpieces, and the tool life is increased by 44%. This verification result has a great significance for improving tool utilization and reducing production cost.

Figure 14 shows the machined surface roughness of the 40th housing. The surface roughness of the housing produced by Tool 1 is the highest, whilst the surface roughness of the housing produced by Tool 3 is the lowest. When the machining parameters are the same, the roughness of the machining surface is determined by the wear condition of the tool nose, so this part of the data is consistent with the above flank wear. Through the working condition verification, after EMCT, the tool hardness increases, the wear consumption slows down, the surface roughness of the housing decreases, and the machining quality is improved.

## 4. Conclusions

In this study, the electromagnetic coupling treatment was carried out on the carbide-coated tool to change the hardness and cutting properties of the tool, this resulted in the extension of tool life and the enhancement of machining quality. The main conclusions are as follows:

- (1) After EMCT, the cutting force on the coated tool decreases. The thermal conductivity of the tool increases and the cutting temperature decreases.
- (2) After EMCT, the coating hardness and plastic deformation resistance are enhanced. The wear is reduced, and workpiece surface roughness is reduced.
- (3) EMCT promotes the migration of elements between coatings, forms the diffusion gradient layer of elements, and improves the adhesion of coatings.
- (4) EMCT with electric field intensity of 1.2 V and magnetic field intensity of 1.0 T can increase tool life by 44% and optimize machining quality.

## Acknowledgments

The authors wish to acknowledge the financial support by the National Natural Science Foundation of China (No. 51705348) and the Science Foundation of Luzhou Government and Sichuan University (No. 2022CDLZ-3 and No.2022CDLZ-14). We would like to appreciate the Analytical & Testing Center of Sichuan University for structural characterization work, and we would be grateful to Aiqun Gu for her help of XRD analysis.

## Disclosure statement

The authors declare that they have no known competing financial interests or relationships that could have appeared to influence the work reported in this paper.

## Funding

The work was supported by the National Natural Science Foundation of China [No. 51705348]; Science Foundation of Luzhou Government and Sichuan University [No. 2022CDLZ-3 and No.2022CDLZ-14].

## Data availability statement

The raw/processed data required to reproduce these findings cannot be shared at this time due to technical or time limitations.

## CRediT authorship contribution statement

Kaien Sun: Methodology; Data curation; Writing original draft.  
Bo Zeng: Conceptualization, Writing original draft, Data curation.  
Yi Qin: Investigation, Validation  
Chengjun Deng: Formal analysis, Software.

Yi Yang: Conceptualization, Data curation.

Kunlan Huang: Validation, Funding acquisition, Writing – review & editing.

Jie Wang: Investigation, Project administration.

## References

- [1] Martinez I, Tanaka R, Yamane Y, et al. Wear mechanism of coated tools in the turning of ductile cast iron having wide range of tensile strength. *Precis eng.* 2017;47:46. doi: [10.1016/j.precisioneng.2016.07.003](https://doi.org/10.1016/j.precisioneng.2016.07.003)
- [2] Martinez I, Tanaka R, Yamane Y, et al. Wear Characteristics of coated carbide tools in the face milling of ductile cast iron. *Key Eng Mater.* 2017;749:178. doi: [10.4028/www.scientific.net/KEM.749.178](https://doi.org/10.4028/www.scientific.net/KEM.749.178)
- [3] Katuku K. Regime features of austempered ductile iron cutting. *J Manuf Process.* 2022;83:374. doi: [10.1016/j.jmapro.2022.09.004](https://doi.org/10.1016/j.jmapro.2022.09.004).
- [4] Yaltese MA, Chaoui K, Zeghib N, et al. Hard machining of hardened bearing steel using cubic boron nitride tool. *J Mater Process Tech.* 2009;209(2):1092. doi: [10.1016/j.jmatprotec.2008.03.014](https://doi.org/10.1016/j.jmatprotec.2008.03.014)
- [5] Wu H, Liu W, Xu Y, et al. Vat photopolymerization-based 3D printing of complex-shaped and high-performance Al<sub>2</sub>O<sub>3</sub> ceramic tool with chip-breaking grooves: cutting performance and wear mechanism. *J Asian Ceram Soc.* 2023;11(1):159. doi: [10.1080/21870764.2023.2168343](https://doi.org/10.1080/21870764.2023.2168343)
- [6] Grzesik W, Rech J, Żak K, et al. Machining performance of pearlitic–ferritic nodular cast iron with coated carbide and silicon nitride ceramic tools. *Int J Mach Tools Manuf.* 2009;49(2):125. doi: [10.1016/j.ijmachtools.2008.10.003](https://doi.org/10.1016/j.ijmachtools.2008.10.003)
- [7] Yigit R, Celik E, Findik F, et al. Tool life performance of multilayer hard coatings produced by HTCVD for machining of nodular cast iron. *Int J Refract Metals Hard Mater.* 2008;26(6):514. doi: [10.1016/j.ijrmhm.2007.12.003](https://doi.org/10.1016/j.ijrmhm.2007.12.003)
- [8] Okada M, Hosokawa A, Tanaka R, et al. Cutting performance of PVD-coated carbide and CBN tools in hardmilling. *Int J Mach Tools Manuf.* 2011;51(2):127. doi: [10.1016/j.ijmachtools.2010.10.007](https://doi.org/10.1016/j.ijmachtools.2010.10.007)
- [9] Camuşcu N. Effect of cutting speed on the performance of Al<sub>2</sub>O<sub>3</sub> based ceramic tools in turning nodular cast iron. *Mater Design.* 2006;27(10):997. doi: [10.1016/j.matdes.2005.02.011](https://doi.org/10.1016/j.matdes.2005.02.011)
- [10] Eraslan D, Balci A, Çetin B, et al. Machinability evaluations of austempered ductile iron and cast steel with similar mechanical properties under eco-friendly milling conditions. *J Mater Res Technol.* 2021;11:1443. doi: [10.1016/j.jmrt.2021.01.123](https://doi.org/10.1016/j.jmrt.2021.01.123)
- [11] Yuan M, Wang J, Wang M, et al. Enhanced carbide tool life by the electromagnetic coupling field for sustainable manufacturing. *Int J Adv Manuf Technol.* 2020;108(11–12):3905. doi: [10.1007/s00170-020-05612-3](https://doi.org/10.1007/s00170-020-05612-3)
- [12] Wang L, Yuan M, Li Y, et al. Cutting mechanism of WC-8Co cemented carbide for dry turning of Ti<sub>6</sub>Al<sub>4</sub>V before and after pulsed electromagnetic coupling processing. *Rare Metal Mater Eng.* 2020;49:4016.
- [13] Wang Z, Huang Y, Guo W, et al. Effects of pulsed magnetic field on the flight and impact of supersonic plasma spraying particles and the properties of coatings. *Mater Design.* 2022;223:111127. doi: [10.1016/j.matdes.2022.111127](https://doi.org/10.1016/j.matdes.2022.111127)
- [14] Yang Y, Qin Y, Yang Y, et al. Enhancing the wear resistance of a cemented carbide/titanium alloy

- under magnetofluid lubrication via the magnetic response. *Wear.* 2022;500-501:204370. doi: 10.1016/j.wear.2022.204370
- [15] Yang Y, Yang Y, Li Q, et al. An eco-friendly pulsed magnetic field treatment on cemented carbide (WC-12Co) for enhanced milling performance. *J Clean Prod.* 2022;340:130748. doi: 10.1016/j.jclepro.2022.130748.
- [16] Li Q, Yang Y, Yang Y, et al. Enhancing the wear performance of WC-6Co tool by pulsed magnetic field in Ti-6Al-4V machining. *J Manuf Process.* 2022;80:898. doi: 10.1016/j.jmapro.2022.06.054
- [17] Qu H, Zhang L, Chen Z, et al. Pulsed magnetic field treatment of TiAlSiN-coated milling tools for improved cutting performances. *Int J Adv Manuf Technol.* 2022;120(9-10):6723. doi: 10.1007/s00170-022-09145-9
- [18] Fei H, Wu H, Yang X, et al. Pulsed magnetic field treatment of cBN tools for improved cutting performances. *J Manuf Process.* 2021;69:21. doi: 10.1016/j.jmapro.2021.07.036
- [19] Shi L, Zou J, Sun L, et al. Effect of electropulsing treatment on microstructure and mechanical properties of Cu-20Ni-20Mn alloy. *Mater Sci Eng A.* 2022;855:143847. doi: 10.1016/j.msea.2022.143847.
- [20] Lu Z, Guo C, Li P, et al. Effect of electropulsing treatment on microstructure and mechanical properties of intermetallic Al<sub>3</sub>Ti alloy. *J Alloy Compd.* 2017;708:834. doi: 10.1016/j.jallcom.2017.03.085
- [21] Zhang Q, Huang K, Wang J, et al. Effect of pulse electromagnetic coupling treatment on thermal conductivity of WC-8Co cemented carbide. *Ceram Int.* 2021;47(16):22683. doi: 10.1016/j.ceramint.2021.04.283
- [22] Yuan M, Wang J, Wang L, et al. Electromagnetic coupling field strengthening of WC-TiC-Co cermet tools. *Ceram Int.* 2021;47(3):3747. doi: 10.1016/j.ceramint.2020.09.232
- [23] Meng Y, Deng J, Wu J, et al. Improved interfacial adhesion of AlTiN coating by micro-grooves using ultrasonic surface rolling processing. *J Mater Process Tech.* 2022;304:117570. doi: 10.1016/j.jmatprotec.2022.117570
- [24] Cui Z, Ni J, He L, et al. Investigation of chip formation, cutting force and surface roughness during orthogonal cutting of polytetrafluoroethylene. *J Manuf Process.* 2022;77:485. doi: 10.1016/j.jmapro.2022.03.031
- [25] Zhao J, Liu Z. Influences of coating thickness on cutting temperature for dry hard turning Inconel 718 with PVD TiAlN coated carbide tools in initial tool wear stage. *J Manuf Process.* 2020;56:1155. doi: 10.1016/j.jmapro.2020.06.010.
- [26] Chang K, Dong Y, Zheng G, et al. Friction and wear properties of TiAlN coated tools with different levels of surface integrity. *Ceram Int.* 2022;48(4):4433. doi: 10.1016/j.ceramint.2021.10.105
- [27] You Q, Xiong J, Li H, et al. Study on the microstructure and high temperature friction and wear characteristics of three CVD coated cermets. *Int J Refract Metals Hard Mater.* 2021;96:105495. doi: 10.1016/j.ijrmhm.2021.105495
- [28] Skordaris G, Bouzakis KD, Kotsanis T, et al. Effect of PVD film's residual stresses on their mechanical properties, brittleness, adhesion and cutting performance of coated tools. *CIRP J Manuf Sci Technol.* 2017;18:145. doi: 10.1016/j.cirpj.2016.11.003
- [29] Breidenstein B, Denkena B. Significance of residual stress in PVD-coated carbide cutting tools. *CIRP Ann.* 2013;62(1):67. doi: 10.1016/j.cirp.2013.03.101
- [30] Leyland A, Matthews A. On the significance of the H/E ratio in wear control: a nanocomposite coating approach to optimised tribological behaviour. *Wear.* 2000;246(1-2):1. doi: 10.1016/S0043-1648(00)00488-9
- [31] Qu J, Riester L, Shih AJ, et al. Nanoindentation characterization of surface layers of electrical discharge machined WC-Co. *Materials Science & Engineering A, Structural Materials: Properties, Microstructure And Processing.* 2003;344(1-2):125. doi: 10.1016/S0921-5093(02)00395-7
- [32] Beake BD. The influence of the H/E ratio on wear resistance of coating systems – insights from small-scale testing. *Surf Coat Technol.* 2022;442:128272. doi: 10.1016/j.surfcoat.2022.128272.
- [33] You Q, Xiong J, Li H, et al. Structure and mechanical behavior evaluation of CVD multilayer coatings deposited on Ti(C,N)-based cermets. *Ceram Int.* 2022;48(9):13250. doi: 10.1016/j.ceramint.2022.01.203
- [34] Doğan F, Uysal M, Duru E, et al. Pulsed electrodeposition of ni-B/TiN composites: effect of current density on the structure, mechanical, tribological, and corrosion properties. *J Asian Ceram Soc.* 2020;8(4):1271. doi: 10.1080/21870764.2020.1840704
- [35] Bobzin K, Brögelmann T, Maier HJ, et al. Influence of residual stresses in hard tool coatings on the cutting performance. *J Manuf Process.* 2021;69:340. doi: 10.1016/j.jmapro.2021.08.011
- [36] Chellappa M, Vijayalakshmi U. Improved corrosion resistant and mechanical behavior of distinct composite coatings (silica/titania/zirconia) on Ti-6Al-4V deposited by EPD. *J Asian Ceram Soc.* 2017;5(3):326. doi: 10.1016/j.jascer.2017.06.005
- [37] Ma D, Xue Y, Gao J, et al. Effect of Ta diffusion layer on the adhesion properties of diamond coating on WC-Co substrate. 2020;527:146727. doi: 10.1016/j.apsusc.2020.146727
- [38] Zoestbergen E, van de Langkruis J, Maalman TFJ, et al. Influence of diffusion on the coating adhesion of zinc-magnesium thin films onto steel. *Surf Coat Technol.* 2017;309:904. doi: 10.1016/j.surfcoat.2016.10.063
- [39] Böttcher CJF, van Belle OC, Bordewijk P, et al. Theory of electric polarization. *J Electrochem Soc.* 1974;121(6):211C. doi: 10.1149/1.2402382
- [40] Pan R, Wang Q, Sun D, et al. Effects of electric field on interfacial microstructure and shear strength of diffusion bonded  $\alpha$ -Al<sub>2</sub>O<sub>3</sub>/Ti joints. *J Eur Ceram Soc.* 2015;35(1):219. doi: 10.1016/j.jeurceramsoc.2014.07.025
- [41] Hu D, Chen J, Su Z, et al. Critical electric field stabilizing structure of Al<sub>2</sub>O<sub>3</sub>/TiO<sub>2</sub>/Al<sub>2</sub>O<sub>3</sub> thin film for achieving high energy density. *Ceram Int.* 2023;49(11):17296. doi: 10.1016/j.ceramint.2023.02.096
- [42] Young L. Anodic oxide films. London; New York: Academic Press; 1961.
- [43] Qian C, Liu Q, Xiong X, et al. Mechanism for magnetic field induced structural relaxation and accompanying fracture toughness improvement of the thermal spraying coating. *Mater Design.* 2022;223:111113. doi: 10.1016/j.matdes.2022.111113
- [44] Grzesik W, Małeczka J. Documentation of tool wear progress in the machining of nodular ductile iron with silicon nitride-based ceramic tools. *CIRP Ann.* 2011;60(1):121. doi: 10.1016/j.cirp.2011.03.083